J. Chem. Sci. Vol. 128, No. 3, March 2016, pp. 357–363.
DOI 10.1007/s12039-015-1024-6

Facile growth of Ag@Pt bimetallic nanorods on electrochemically reduced graphene oxide for an enhanced electrooxidation of hydrazine

S E JEENA and T SELVARAJU*
Department of Chemistry, Karunya University, Coimbatore 641 114, India
e-mail: selvaraju@karunya.edu

MS received 16 July 2015; revised 8 December 2015; accepted 8 December 2015

Abstract. An efficient transducer was constructed by the direct growth of bimetallic Ag@Pt nanorods (NRDs) on L−tryptophan functionalized electrochemically reduced graphene oxide (L−ERGO) modified electrode using galvanic displacement method for the electrooxidation of hydrazine. Initially, one dimensional bimetallic Ag@Cu core−shell NRDs were grown on L−ERGO modified electrode by simple seed mediated growth method. Then, the Cu shells at bimetallic NRDs were exchanged by Pt through galvanic displacement method. Accordingly, the synergetic effect produced by the combination of Ag and Pt as NRDs at L−ERGO surface enabled an enhancement in the electrocatalytic efficiency for hydrazine oxidation. L−ERGO supported bimetallic Ag@Pt NRDs were characterised by scanning electron microscopy (SEM), energy dispersive X-ray spectroscopy (EDX) and cyclic voltammetric techniques. Finally, the modified electrode was successfully used for the electrooxidation of hydrazine in PB (pH 7.4) with a detection limit of 6×10^{-7} M (S/N =3). Importantly, the presence of Pt on Ag surface plays a vital role in the electrooxidation of N_2H_4 at −0.2 V with an onset potential at −0.5 V where its overpotential has decreased. On the other hand, L−ERGO nanosheets tend to facilitate an effective immobilization of low density Ag seeds (Ag_{seeds}) on its surface. Chronoamperometric studies were used to study the linear correlation of [N_2H_4] between 1 mM and 10 mM. The modified electrode shows a high sensitivity and selectivity for a trace amount of N_2H_4 in the presence of different interfering cations and anions.

Keywords. Electrochemically reduced graphene oxide nanosheets; bimetallic Ag@Pt nanorods; seed mediated growth method; galvanic displacement and hydrazine.

1. Introduction

Hydrazine is a commonly known mutogenic, heptotoxic, and carcinogenic substance with adverse health effects.[1,2] It is widely used for various applications such as antioxidants, corrosion inhibitors, propellants and in agricultural fields.[3,4] Instead, the acute exposure to hydrazine damages the kidney, liver and DNA.[5] According to the environmental protection agency (EPA), the optimum level of hydrazine should be 0.1 ppm in industrial and in agricultural effluents.[6] Due to its toxicity and industrial significance, the accurate determination of hydrazine in sub-micromolar level is getting wider attention. Even though various techniques were available for hydrazine sensing such as spectrophotometry, ion chromatography, chemiluminescence and titrimetry, nanomaterials based electrochemical methods received much attention due to its simplicity, wide linear range, better sensitivity and fast response.[7–11] In contrast, the electrooxidation of hydrazine at conventional carbon electrodes are relatively slow and possess high overpotential.[12] Mostly, transition metal nanoparticles such as Ag, Au, Cu, Pt and Pd based on its size and shape show excellent electrocatalytic property. Wang *et al.,* have developed silver nanocubes modified electrodes as sensing platform for hydrazine and hydrogen peroxide.[13] Li *et al.,* have used gold nanoparticle with polypyrrole nanowire modified glassy carbon electrodes for the electrochemical sensing of hydrazine.[14]

Carbon nanomaterials such as carbon nanotubes, carbon fibres and reduced graphene oxide have been widely used as a better platform for bimetallic nanostructures in various fields.[15,16] Sudip *et al.,* have constructed CNT supported Pt nanoparticles for electrochemical sensing of hydrazine.[17] Fang *et al.,* have electrodeposited AuPdCu alloy nanoparticles on CNT modified electrodes for the electrooxidation of hydrazine.[18] Guang–Wu *et al.,* deposited Ag nanoparticles on CNT for the electrooxidation of hydrazine.[19] Alternatively, reduced graphene oxide has several advantages over other carbon materials due to its excellent conductivity and large surface area.[20] Cong *et al.,*

*For correspondence
Dedicated to Professor R. Ramaraj on the occasion of his 60th birth anniversary.

used poly(sodium styrenesulfonate) graphene oxide nanocomposites film for the amperometric sensing of hydrazine.[21]

Even though different methods were available for the growth of nanomaterials on reduced graphene oxide surface,[22,23] the direct growth of one dimensional Ag based bimetallic nanostructures on ERGO by galvanic replacement method is not explored extensively. In the present work, we have developed a low cost and an efficient seed mediated growth followed by galvanic replacement for the direct growth of bimetallic Ag@Pt NRDs on L−ERGO surface. Poor dispersion quality of reduced graphene oxide is the main challenge in the chemical method. It will be overcome by the electrochemical reduction of graphene oxide on electrode surface. In the next step, surface functionalization plays a prominent role for the direct growth of one dimensional nanostructure on ERGO. It is carried out using L−tryptophan as a functionalizing agent for tuning the growth of bimetallic NRDs on ERGO surface.[24] First, Ag@Cu core−shell bimetallic NRDs on L−ERGO surface has been developed by seed mediated growth method and the shell like Cu is replaced by Pt using galvanic replacement reaction. It is achieved by the difference in the standard reduction potential which is the driving force for the galvanic replacement reaction between Cu^{2+}/Cu ($E^\circ = +0.3$ V) and Pt^{4+}/Pt ($E^\circ = 1.44$ V). Ultimately, two key aspects are to be identified such as (1) The synergetic effect between the metals at bimetallic NRDs and (2) the large surface area of ERGO. The synergetic effect is due to an interaction between Ag and Pt at the bimetallic NRDs, and the resultant enhancement in the effective loading of bimetallic NRDs might reflect its large surface area of L−ERGO. These properties could tend to accelerate its electrocatalytic activity for the direct determination of hydrazine with better reproducibility, high sensitivity and good stability. In addition, the interference of various cations and anions would be explored in the presence of hydrazine at the newly developed transducer.

2. Experimental

2.1 *Materials*

Graphite powder (300 mesh) was received from Alfa Aesar, UK. Hydrogen peroxide, sulphuric acid, sodium nitrate, copper nitrate, L-tryptophan, sodium borohydride, sodium hydroxide, monosodium dihydrogen phosphate and disodium hydrogen phosphate were purchased from Merck, India. Cetyl trimethyl ammonium bromide (CTAB) and hydrazine were obtained from Himedia, India. Platinum (IV) chloride, ascorbic acid (AA), trisodium citrate and silver nitrate were obtained from Sigma-Aldrich, USA. All reagents were of analytical grade and used without further purification. All solutions were prepared using deionized (DI) water.

2.2 *Characterizations*

In order to study the morphological and structural properties, L−ERGO nanosheets supported bimetallic Ag@Pt NRDs were grown on Indium Tin Oxide (ITO) electrode surface. Prior to surface modification, ITO plates were cleaned and pretreated with a mixture of H_2O, H_2O_2 and NH_4OH in the ratio of 5:1:1. The surface morphologies of bimetallic Ag@Pt NRDs on L−ERGO nanosheets were confirmed by SEM (VEGA 3 TESCAN, USA) analyses. EDX (Bruker, Germany) analysis was used to confirmed the presence of metallic Ag and Pt.

2.3 *Electrochemical measurements*

All electrochemical measurements were studied using CHI 660D electrochemical workstation (CH Instruments, USA). The electrochemical cell consists of a three electrode setup, where Ag@Pt NRDs/L−ERGO modified glassy carbon electrode (0.07 cm^2) was used as working electrode, Ag/AgCl filled with a saturated KCl solution as the reference electrode, and platinum wire as a counter electrode.

2.4 *Synthesis of bimetallic Ag@Pt NRDs on L-ERGO nanosheets*

Glassy carbon electrodes (GCE) were polished well with alumina powder (0.3 micron) using buehler cloth, sonicated in ethanol-water mixture for 4 min, washed with DI water and finally dried at room temperature. Graphene oxide (GO) was synthesised by the modified Hummers method.[25] Then, 10 μl of exfoliated GO dispersion was drop casted on GCE and dried for 1 h at r.t. Afterwards, GO was subjected to reduce electrochemically in the potential range between 0.0 and −1.5 V in 0.05 M phosphate buffer (pH 5) for 30 continuous cycles.[26] In the first cycle, a prominent reduction peak appeared at −1.15 V due to reduction of oxygen functional groups on GO surface. After a few cycles, the reduction peak disappeared, which indicates the complete reduction of GO to ERGO. Then, the ERGO/GCE was dipped in L−tryptophan (1 mg/ml) for 24 h at r.t. for effective surface functionalization.

Subsequently, bimetallic Ag@Pt NRDs were generated on L−ERGO surface by galvanic replacement

method. First, Ag@Cu NRDs were grown on L−ERGO surface by seed mediated growth approach.[24,27] Then, Ag@Cu NRDs/L−ERGO/GCEs were dipped in 2.4 mM $PtCl_4$ for 95 sec where galvanic replacement of Cu by Pt surface has occured spontaneously. As a result, the modified electrode was developed with Pt shell would be indicated as Ag@Pt NRDs/L−ERGO/GCE.

3. Results and Discussion

3.1 *Surface characterization*

Bimetallic Ag@Pt NRDs were directly grown on L−ERGO nanosheets by seed mediated growth method according to scheme 1. It shows the growth of Ag_{seeds} into bimetallic Ag@Cu NRDs and subsequently the shell like Cu has exchanged by Pt using galvanic replacement method at L−ERGO nanosheets surface. Figure 1 displays the SEM images of ERGO (A) and Ag@Pt NRDs decorated L−ERGO (B) nanosheets.

Figure 1A exhibits wrinkled sheet like morphology of ERGO nanosheets on the electrode surface which provides a very large surface area.[21] Figure 1B clearly shows the successful growth of Ag@Pt NRDS on L−ERGO surface with a diameter of 180 ± 2 nm. Recently, SEM image of Ag@Cu NRDs on L−ERGO surface has been reported elsewhere.[24] Further, EDX measurement (figure S1) confirmed the existence of both Ag and Pt at bimetallic NRDs on the electrode surface. In addition, cyclic voltammogram (CV) confirmed the existence of Pt at bimetallic Ag@Pt NRDs on L−ERGO surface where a typical voltammetric characteristics of metallic Pt in 0.5 M H_2SO_4 was observed. A broad peak in the range of −0.3 to 0.1 V which was accounted for metallic Pt surface associated with the hydrogen adsorption/desorption process (Figure not shown). Importantly, there was no oxidative peak around 0.23 V in 0.5 M H_2SO_4 which mainly attributed the restriction of Ag dissolution. This property solely indicates the complete coverage of Pt layer at bimetallic Ag@Pt NRDs. Also, it is a distinct evidence of the presence of Pt over Ag surface at Ag@Pt NRDs/L−ERGO/GCE.

The electrochemical surface area of Pt at bimetallic NRDs modified electrode was calculated in 0.5 mM $K_4Fe(CN)_6$ by chronocoulometry where the charge (Q) was measured as a function of time.[28] Figure S2 shows Anson plot where a linear relationship between Q and the square root of time ($t^{\frac{1}{2}}$) was measured. From the

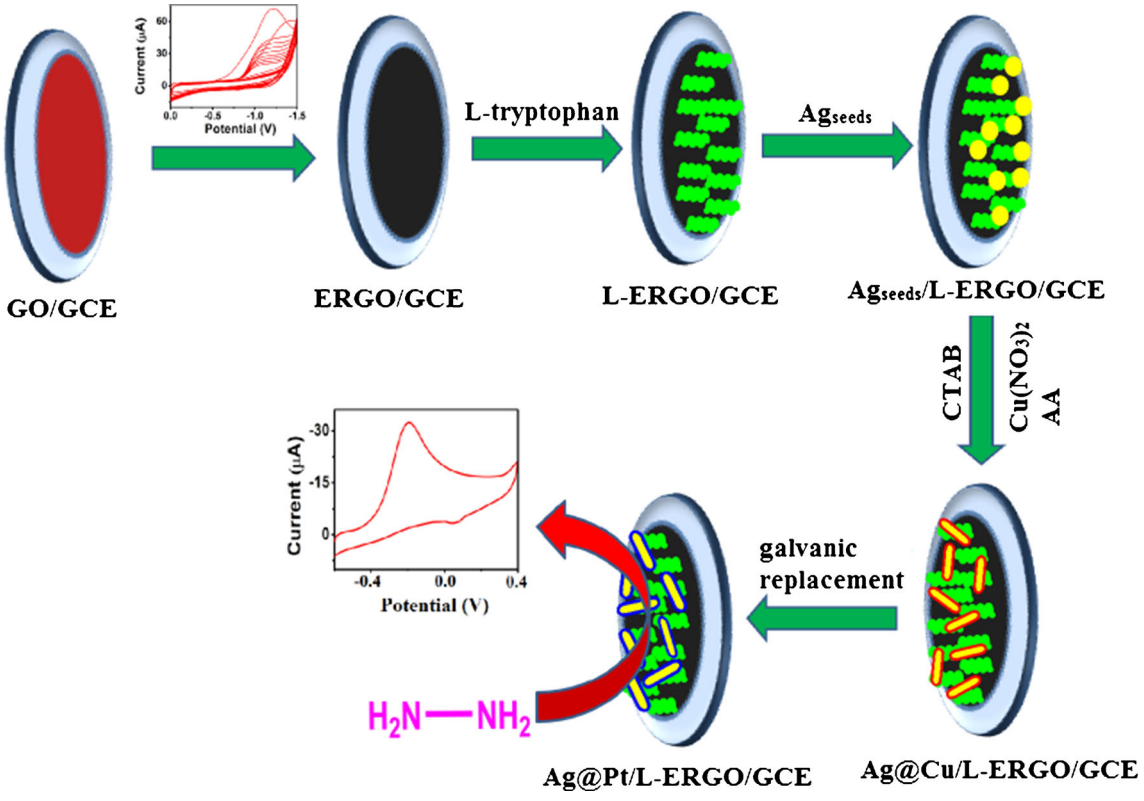

Scheme 1. Schematic representation of 1D growth of bimetallic Ag@Pt NRDs on L− tryptophan functionalized ERGO nanosheets at the GCE surface.

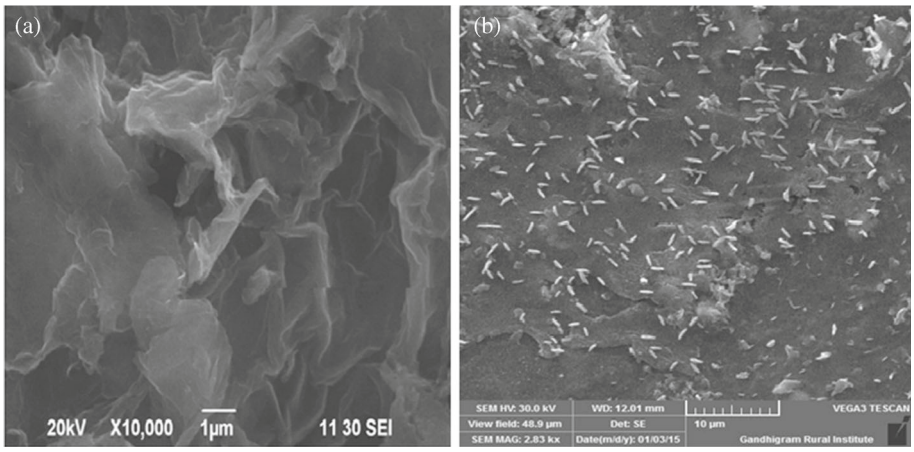

Figure 1. SEM images of ERGO (a) and Ag@Pt NRDs decorated at L−ERGO (b).

slope of Anson plot (a), the electrochemical surface area (A) was calculated as 0.46 cm^{-2} which coincides with the CV results.

$$A = a/\left(2nFCD^{1}/2/\pi^{1}/2\right) \quad (1)$$

Here F is the Faraday's constant, D is diffusion coefficient and C is the concentration of analyte.

3.2 *Electrocatalytic oxidation of hydrazine at L-ERGO supported Ag@Pt NRDs electrode*

The electrooxidation of N_2H_4 was investigated at L−ERGO supported bimetallic Ag@Pt NRDs electrode. Figure 2 shows the CV response of bimetallic Ag@Pt/L−ERGO/GCE (a) in 0.5 mM N_2H_4 in PB (pH 7.4). In the presence of N_2H_4, an enhanced oxidative peak current was observed at −0.2 V, whereas no such oxidative peak was observed in the absence of N_2H_4 (figure 2 (inset)). For comparison, N_2H_4 electrooxidation was also carried out at bimetallic Ag@Cu/L−ERGO/GCE (b), Ag_{seeds}/L−ERGO/GCE (c) and at bare GCE (d) under identical conditions. No observable electrooxidative peak current was noticed at these electrodes in the potential between −0.6 V and 0.4 V. Thus, the existence of Pt surface over Ag plays a synergistic role in the electrocatalytic oxidation of N_2H_4 at Ag@Pt NRDs/L−ERGO/GCE. In general, Pt nanoparticles have been considered as an active electrocatalyst for the oxidation of N_2H_4.[17] On the other hand, a major setback at Pt nanoparticles modified electrode surfaces were identified as kinetic limitation which leads to a high overpotential for the oxidation of N_2H_4. In the present investigation, it is overcome by the formation of bimetallic Ag@Pt NRDs at L−ERGO. Here, the heterometallic bonding interactions (ligand effect) between the metals such as Ag and Pt resulted in the enhancement of catalytic properties for N_2H_4 electrooxidation. Eventually, L−ERGO provides a very large electrode surface area which facilitates and favors the electron transfer for N_2H_4 oxidation. Accordingly, L−ERGO supported bimetallic Ag@Pt NRDs electrode shows an excellent electroactivity for the oxidation of N_2H_4 with a very low onset potential at −0.5 V.

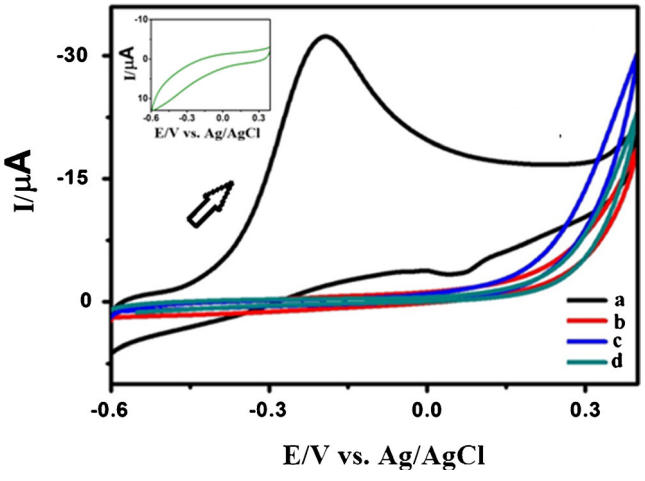

Figure 2. CVs of Ag@Pt/L−ERGO/GCE (a), Ag@Cu/L−ERGO/GCE (b), Ag_{seeds}/L−ERGO/GCE (c) and bare GCE (d) in the presence of 0.5 mM N_2H_4 in PB (pH 7.4). Inset: CV of Ag@Pt/L−ERGO/GCE in PB (pH 7.4).

The effect of scan rate for the electrooxidation of N_2H_4 at Ag@Pt/L−ERGO/GCE was investigated to understand the electron transfer kinetics of the electrode process. Figure 3A shows the CVs of Ag@Pt/L-ERGO/GCE in 0.5 mM N_2H_4 under different scan rate from 0.01 to 0.1 V/s. It shows a positive shift in the oxidation potential with respect to increase in scan rate. Figure 3B shows a linear relationship between the anodic peak current and the square root of scan rate with the linear regression equation $I_{pa} = 61.057$ (V/s^{-1})

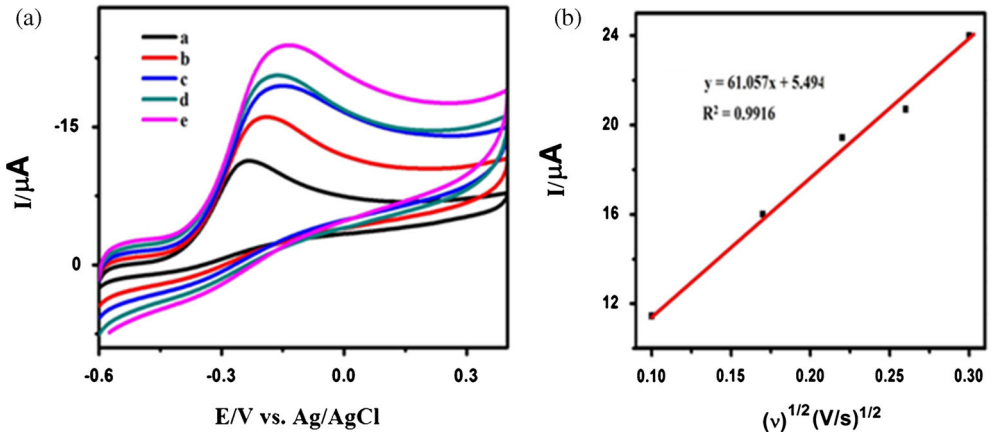

Figure 3. (**a**) CVs of Ag@Pt/L−ERGO/GCE in 0.5 mM in N_2H_4 in PB (pH 7.4) at 0.01 (a), 0.03 (b), 0.05 (c), 0.07 (d) and 0.09 (e) V s^{-1} and; (**b**) Plot of the peak currents vs. square root of scan rate.

+ 5.494. The linear increase in the anodic peak current with respect to the square root of scan rate indicates that the electrooxidation of N_2H_4 at Ag@Pt/L−ERGO/GCE is a diffusion controlled process. The oxidation of N_2H_4 depends on the electrolyte and the nature of the electrodes. At pH 7.4, N_2H_4 exists in unprotonated form and involve two steps process during the course of electrooxidation

$$N_2H_4 + H_2O \longrightarrow N_2H_3 + H_3O^+ + e^- \qquad (2)$$

$$N_2H_3 + H_2O \longrightarrow N_2H_3 + 3H_3O^+ + 3e^- \qquad (3)$$

Eq. 2 is the rate determining step involves a one electron transfer process and the electron transfer coefficient has been estimated as 0.52 from the equation

$$(1-\alpha)n_\alpha = \frac{47.7\,\text{mV}}{E_p - E_{p/2}} \qquad (4)$$

Further, the total number of electrons transferred in the electrooxidation of N_2H_4 was calculated using the equation for an irreversible system.[29]

$$Ip = 3.01 \times 10^5 n\,[(1-\alpha)\,n_\alpha]^{1/2}\,ACD^{1/2}\nu^{1/2} \qquad (5)$$

Here D is the diffusion coefficient of the electroactive species, C is the concentration of N_2H_4, n the total no. of electrons transferred and $\nu^{1/2}$ is the square root of scan rate. Hence, the number of electrons transferred is calculated as 5 using the diffusion coefficient as 2.4 × 10^{-5} cm^2 s^{-1} for N_2H_4.[11,14]

The effect of pH on the electrooxidation of N_2H_4 with respect to anodic peak current and peak potential were investigated at Ag@Pt/L−ERGO/GCE. Figure 4A shows the variation in the oxidation peak potential with respect to pH between pH 5.4 and 9.4. From pH 5.4 to 7.4, a linear negative shift in the oxidation peak potential was observed with an equation y = −0.1673x + 1.0502 (R^2 = 0.983). In contrast, a slight positive shift in the peak potential was observed from 7.4 to 9.4. From the slope of oxidation peak potential *vs.* pH using the equation dE/dpH = 0.059X/αn, the number of exchanged protons were estimated as 4.5. Here, α is the electron transfer coefficient and n is the number of electrons. This indicates that a proton has been transferred for each electron in the electrooxidation of N_2H_4. Figure 4B shows the variation of oxidative peak current at different pH. The oxidative peak current for N_2H_4 has increased from 5.4 to 7.4 and then decreased at 8.4 or at 9.4. It is due to the pKa of N_2H_4 (7.9) where it exists in the protonated or deprotanted form and is less active at low or high pH. This leads to low oxidation current at pH less than or greater than 7.4. Therefore, pH 7.4 was optimized for all the experimental studies.

Ag@Pt/L−ERGO/GCE was used to construct an amperometric sensor for N_2H_4. Figure 5A shows the chronoamperometric current response for the successive addition of an aliquot of N_2H_4 after every 40 s in PB (pH 7.4). It exhibits a steady increase in the oxidation current for [N_2H_4] between 1 mM and 10 mM. Figure 5B shows a linear increase in the oxidative current for [N_2H_4] with an equation, I_{pa} = 2.417 [N_2H_4] + 24.647 (R^2 = 0.995). The detection limit of N_2H_4 was estimated as 6 × 10^{-7} M with a signal to noise ratio 3 (S/N=3) at Ag@Pt/L−ERGO/GCE. In addition, the interference study of a 100 fold higher concentration of different cations and anions such as Li^+, Na^+, K^+, Ca^{2+}, Mg^{2+}, Cl^-, PO_4^{3-}, CO_3^{2-}, NO_3^- and SO_4^{2-} were carried out in the presence of 5 μM N_2H_4 using chronoamperometry. Accordingly, the aforementioned ions did not interfere in the electrochemical

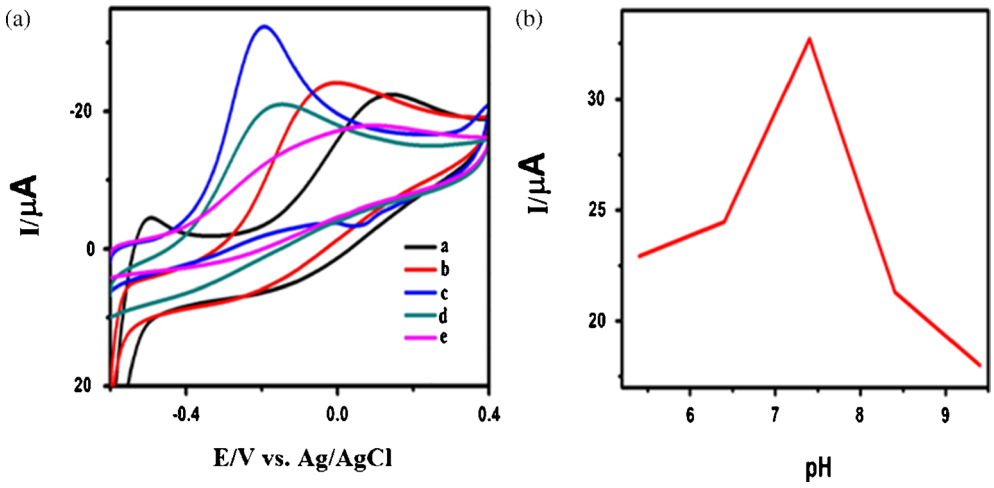

Figure 4. (**a**) CVs of Ag@Pt/L−ERGO/GCE at different pH for 0.5 mM N_2H_4 [pH: 5.4 (a), 6.4 (b), 7.4 (c), 8.4(d) and 9.4(e)] and; (**b**) plot of pH vs anodic peak current.

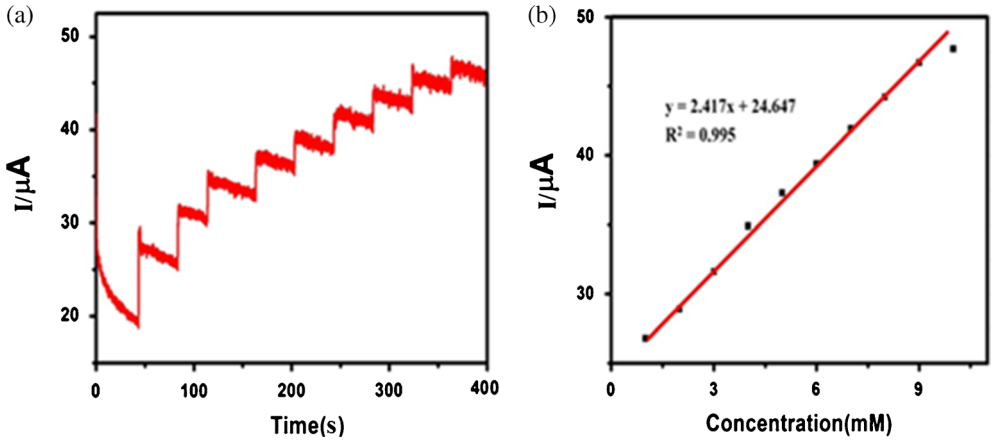

Figure 5. (**a**) Chronoamperometric response of Ag@Pt/L-ERGO/GCE from 1 mM to 10 mM [N_2H_4] in PB (pH 7.4). The electrode potential is fixed at -0.2 V and; (**b**) Plot of [N_2H_4] vs anodic peak currents.

oxidation and in the accurate determination of N_2H_4 at Ag@Pt/L−ERGO/GCE. The stability and reproducibility of L−ERGO supported bimetallic Ag@Pt NRDs electrodes were also investigated by CV. After 20 continuous cycles, Ag@Pt/L−ERGO modified electrode shows a very good response for N_2H_4 electrooxidation with relative standard deviation (RSD) of 2.9%. Further, the modified GCE was stored and studied after 5 weeks at r.t. where it exhibits a similar current response for N_2H_4 electrooxidation under identical conditions.

4. Conclusions

In the present study, an efficient voltammetric sensor for N_2H_4 using L−ERGO supported bimetallic Ag@Pt NRDs electrode was constructed satisfactorily. Bimetallic Ag@Pt NRDs were directly grown on L−ERGO surface by seed mediated followed by galvanic replacement method. SEM image shows the successful growth of bimetallic Ag@Pt NRDs with a size distribution of 180 nm on the suface of ERGO nanosheets. Further, EDX pattern authenticated the presence of metallic Ag and Pt at ERGO surface. Finally, the developed transducer exhibits a high sensitivity and good detection limit for the electrochemical oxidation of N_2H_4 with decreased overpotential. The synergetic effect were produced due to the coexistence of new generation material such as galvanically replaced bimetallic Ag@Pt NRDs at L−ERGO surface for an enhanced electrocatalytic oxidation of N_2H_4.

Supplementary Information (SI)

Supplementary Information associated with this article is available at www.ias.ac.in/chemsci.

Acknowledgements

Financial support by DST-SERB, New Delhi (File No. SR/FT/CS-44/2011 dated 04.05.2012) is gratefully acknowledged. We thank Karunya University, Coimbatore for providing instrumental facilities.

References

1. Golabi S M and Zare H R 1999 *J. Electroanal. Chem.* **465** 168
2. Garrod S, Bollard M E, Nicholls A W, Connor S C, Connelly J, Nicholson J K and Holmes E 2005 *Chem. Res. Toxicol.* **18** 115
3. Ahmad U, Rahman M M and Hahn Y B 2009 *Talanta* **77** 1376
4. Umar A, Rahman M M, Kim S H and Hahn Y B 2008 *Chem. Commun.* **2** 166
5. Amlathe S and Gupta V K 1988 *Analyst* **113** 1481
6. Kim S K, Jeong Y N, Ahmed M S, You J M, Choi H C and Jeon S 2011 *Sens. Actuators*, *B* **153** 246
7. Safavi A, Abbasitabar F and Nezhad M R H 2007 *Chem. Anal.* **52** 835
8. Mori M, Tanaka K, Xu Q, Ikedo M, Taoda H and Hu W 2004 *J. Chromatogr. A* **11** 1039
9. Collins G E, Latturner S and Rose-Pehrsson S L 1995 *Talanta* **42** 543
10. Budkuley J S 1992 *Microchim. Acta* **108** 103
11. Li J, Xie H and Chen L 2011 *Sens. Actuators*, *B* **153** 239
12. Zhang C, Wang G, Ji Y, Liu M, Feng Y, Zhang Z and Fang B 2010 *Sens. Actuators*, *B* **150** 247
13. Wang Y, Yang X, Bai J, Jiang X and Fan G 2013 *Biosens. Bioelectron.* **43** 180
14. Li J and Lin X 2007 *Sens. Actuators, B* **126** 527
15. Pumera M 2010 *Chem. Soc. Rev.* **39** 4146
16. Wang X 2005 *Electroanalysis* **17** 7
17. Chakraborty S and Retna Raj C 2010 *Sens. Actuators, B* **147** 222
18. Xu F, Zhao L, Zhao F, Deng L, Hu L and Zeng Baizhao 2014 *Int. J. Electrochem. Sci.* **9** 2832
19. Yang G W, Gao G Y, Wang C, Xu C L and Li H L 2008 *Carbon* **46** 747
20. Kamat P V 2010 *J. Phys. Chem. Lett.* **1** 520
21. Wang C, Zhang L, Guo Z, Xu J, Wang H, Zhai K and Zhuo X 2010 *Microchim. Acta* **169** 1
22. Lee M S, Lee K, Kim S Y, Lee H, Park J, Choi K H, Kim H K, Kim D G, Lee D Y, Nam X Y and Park J U 2013 *Nano Lett.* **13** 2814
23. Luo Z, Yuwen L, Bao B, Tian J, Zhu X, Weng L and Wang L 2012 *J. Mater. Chem.* **22** 7791
24. Jeena S E, Gnanaprakasam P, Dakshinamurthy A and Selvaraju T 2015 *RSC Adv.* **5** 48236
25. Gnanaprakasam P and Selvaraju T 2014 *RSC Adv.* **4** 24518
26. Cheemalapati S, Palanisamy S and Chen S M 2013 *Int. J. Electrochem. Sci.* **8** 3953
27. Easow J S and Selvaraju T 2013 *Electrochim. Acta* **112** 648
28. Fragkou V, Ge Y, Steiner G, Freeman D, Bartetzko N and Turner A P F 2012 *Int. J. Electrochem. Sci.* **7** 6214
29. Hubbard A T 1969 *J. Electroanal. Chem.* **22** 165